crystals

MDPI

Article

Novel Organotin(IV) Complexes of 2-[4-Hydroxy-3-((2-hydroxyethylimino)methyl)phenylazo]benzoic Acid: Synthesis, Structure, Noncovalent Interactions and In Vitro Antibacterial Activity

Pratima Debnath [1], Paresh Debnath [1], Manojit Roy [1,*], Lesław Sieroń [2], Waldemar Maniukiewicz [2,*], Tamanna Aktar [3], Debasish Maiti [3], Alexander S. Novikov [4,5,*] and Tarun Kumar Misra [1,*]

1 Department of Chemistry, National Institute of Technology Agartala, Jirania 799046, Tripura, India
2 Institute of General and Ecological Chemistry, Lodz University of Technology, Zeromskiego 116, 90-924 Lodz, Poland
3 Department of Human Physiology, Tripura University, Agartala 799022, Tripura, India
4 Institute of Chemistry, Saint Petersburg State University, Universitetskaya Nab., 7/9, 199034 Saint Petersburg, Russia
5 Research Institute of Chemistry, Peoples' Friendship University of Russia (RUDN University), Miklukho-Maklaya Street, 6, 117198 Moscow, Russia
* Correspondence: mroychem@gmail.com (M.R.); waldemar.maniukiewicz@p.lodz.pl (W.M.); a.s.novikov@spbu.ru (A.S.N.); tkmisra70@yahoo.com (T.K.M.)

check for updates

Citation: Debnath, P.; Debnath, P.; Roy, M.; Sieroń, L.; Maniukiewicz, W.; Aktar, T.; Maiti, D.; Novikov, A.S.; Misra, T.K. Novel Organotin(IV) Complexes of 2-[4-Hydroxy-3-((2-hydroxyethylimino)methyl) phenylazo]benzoic Acid: Synthesis, Structure, Noncovalent Interactions and In Vitro Antibacterial Activity. *Crystals* **2022**, *12*, 1582. https://doi.org/10.3390/cryst12111582

Academic Editor: Kil Sik Min

Received: 24 October 2022
Accepted: 4 November 2022
Published: 7 November 2022

Publisher's Note: MDPI stays neutral with regard to jurisdictional claims in published maps and institutional affiliations.

Abstract: Three new organotin(IV) complexes, $[Me_3Sn(H_2L)]_2$ (**1**), $Bu_3Sn(H_2L)$ (**2**), and $[(Bu_2Sn(H_2L))_2O]_2$ (**3**) were synthesized by the reaction of 2-[4-hydroxy-3-((2-hydroxyethylimino)methyl)phenylazo]benzoic acid (**H_3L**) with appropriate alkyltin(IV) precursors. The complexes were characterized by elemental analysis, IR, and multinuclear (^1H, ^{13}C and ^{119}Sn) NMR spectroscopy. Further, the complex **1** was analyzed by single-crystal X-ray analysis. It displays a 24-membered cyclic dimeric $Me_3Sn^{IV}(H_2L)$ unit where the ligand act as a bridging framework using its carboxylate-O and phenoxy-O atoms. The Sn(IV) adopts distorted trigonal-bipyramidal geometry. In the solution state, the structures were determined by ^{119}Sn-NMR spectroscopy, and the complexes **1** and **2** have distorted tetrahedral geometry, whereas complex **3** shows distorted trigonal-bipyramidal geometry around the tin centres. The Hirshfeld surface analysis and DFT calculations, together with a topological analysis of the electron density distribution in the crystal structure of complex **1**, indicate that its molecular packing determined by various noncovalent interactions, including stacking and hydrogen bonding. The antibacterial studies of the ligand and the complexes (**1–3**) against gram-negative bacteria *viz. Klebsiella pneumoniae (A),Vibrio cholerae (M)* and *Shigella boydii (Q)* and gram-positive bacteria *viz.Staphylococcus aureus* (J), *Streptococcus pneumonia* (K) are promising and the compounds can be treated as potential common antibacterial materials.

Keywords: organotin(IV) compounds; NMR spectroscopy; crystal structure; cyclic dimeric; noncovalent interactions; antibacterial activity

1. Introduction

The development of organotin(IV) compounds for use in biomedical, industrial, and agricultural applications is attracting significant interest from researchers [1]. They have been commercially used as a homogeneous catalyst for polymeric materials, such as PVC, polyurethanes, silicone polymers, etc. [2]. Because of their specific interactions with the phosphate group of DNA, they have been considered advanced anti-cancer agents [3–7] and the agents for other diseases of proliferation [8–10]. They are distinctive from a stereochemical perspective, displaying monomeric, polymeric or cyclic motifs [11,12]. Nevertheless, coordinated ligands play a vital role in the structural variety of organotin(IV)

compounds. Ligands bearing carboxylate/hydroxo groups with Schiff base imine, azo, or azo-imine functionalities have been extensively investigated [13–17] for their stereochemical motifs and biological applications [18–25].

It has been observed that the cyclic compounds formed by organotin(IV) with ligands containing hydroxy-azo/imino-carboxylate groups at the specific positions are either tetrameric or dimeric forms of Sn(IV) [25–31]. Tetrameric Sn(IV) complexes are found to be 36- to 48-members. They adopt distorted trigonal-bipyramidal geometry regardless of the organo-groups linked to Sn(IV). The ring size and multimeric character of Sn(IV) units are thus controlled by the location of the coordinating sites that are present in a ligand frame. Roy M. et al. [25] reported the 48-membered macrocyclic tetrameric trimethyltin(IV) compound with 4-(2,4-dihydroxy-phenylazo)-benzoic acid, where in respect of the azo group the carboxylate is at 4- and the hydroxyl is at 2′-positions and the ligand is in zwitterionic form. The complex showed very good antidiabetic effectiveness, which overcomes the effectiveness of standard compound acarbose. The ligand, 3-(salicylideneamino)benzoate where the carboxylate is at 3- and the hydroxyl is at 2′-positions in respect of the imino function yielded the 44-membered macrocyclic tetrameric triphenyltin(IV) compound [26]. The compound has shown effective anticancer activity as well. Basu Baul T.S. et al. [27] designed the ligand, 5-[(*E*)-2-(3-pyridyl)-1-diazenyl]-2-hydroxybenzoic acid in which the carboxylate and the hydroxyl groups at the 3- and 4-positions of a phenyl ring are linked with 3′-pyridine through the azo-group. With the triphenyltin(IV) fragment, the ligand produced a 44-membered macrocyclic tetrameric structure employing carboxylate-O and pyridine-N. The research group framed a different ligand in which phenylazo group (having no coordination site) attached at 4-position of the hydroxyl group and 3-position of the (methylidene)aminoacetate group. The ligand in its zwitterionic form produced a 36-membered macrocyclic tetrameric structure with the triphenyltin(IV) fragment [28]. Thus, the ligands with coordination sites (carboxylate, hydroxy) at (4,2′), (3,3′), (3,2′) positions yield tetrameric organotin(IV) complexes. On the other hand, the ligands of type (2,4′), i.e., the carboxylate group at 2-position and the hydroxyl group at 4′-position, with $SnPh_3$ and $SnMe_3$ fragments yielded centrosymmetric dimeric 24-membered macrocyclic organotin(IV) compounds [29,30]. In both cases, there are (methylidene)amino fragments at the ortho-position of the hydroxy-group and unlike the (methylidene)aminoacetate group [28], these were found to be uncoordinated. All of the compounds are bioactive and it could be stated that the polynuclear organotin(IV) compounds are supposed to have higher antitumor activity than that of monomeric ones [31].

In this present contribution, we report synthesis of a new ligand of type (2,4′) with a pendent arm of (methylidene)aminoethyl alcohol at the *ortho*-position and its Sn(IV) complexes with trimethyl-, tributyl- and dibutyl-organotin(IV) precursors. The report includes the crystal structure of the complex of $SnMe_3$ fragment which is a 24-membered macrocyclic centrosymmetric dimer of organotin(IV), establishing our observations of dimeric form with the (2,4′) systems from the literature [29,30]. The Hirshfeld surface analysis and DFT calculations, together with a topological analysis of the electron density distribution, were used for theoretical study noncovalent interactions in the obtained crystal structure. Antibacterial properties of all the compounds against both gram-positive and gram-negative bacteria are also highlighted.

2. Materials and Methods

2.1. Materials

Ethanolamine, salicylaldehyde, trimethyltin(IV) chloride, bis-tri-n-butyltin(IV) oxide, *o*-amino benzoic acid, and dibutyltin(IV) oxide were taken from Merck by purchase process and then used without further purification. Nutrient Agar (Hi-media) was used as culture media for the growth of bacterial species. The analysis for the detection of elemental Carbon, hydrogen and nitrogen analyses was performed on a PerkinElmer 2400 series II instrument. The IR spectra were obtained from Perkin Elmer FTIR spectrophotometer in the range of 4000–400 cm^{-1} using KBr discs. ^{1}H, ^{13}C and ^{119}Sn NMR spectra of ligand and

the complexes were recorded on a Bruker AMX 400 spectrometer measured at 400, 100 and 149 MHz, respectively. Me_4Si was employed as a reference compound set at 0.00 ppm for ^1H- and ^{13}C-chemical shifts while Me_4Sn was used as a reference for ^{119}Sn-chemical shifts set at 0.00 ppm.

2.2. Methods

2.2.1. Synthesis of 2-{4-Hydroxy-3-[(2-hydroxyethylimino)methyl]phenylazo}benzoic Acid (H_3L)

The diazotization of 2-aminobenzoic acid, followed by coupling with salicylaldehyde led 2-(3-formyl-4-hydroxyphenylazo)benzoic acid [30]. It (1.00 g, 3.70 mmol) was then dissolved in toluene (50 mL) and heated for 30 min. To this hot toluene solution, ethanolic solution of ethanolamine (0.226 g, 3.70 mmol) was added dropwise in stirring condition, and the mixture was made to reflux for 3 hrs. After the solid product fully formed, it was filtered out, vacuum-dried, and then again recrystallized from anhydrous methanol to produce the light yellow H_3L product.

Yield: 0.967 g, 83.3%; m.p.: 210–214 °C. Anal.Calcd. for $C_{16}H_{15}N_3O_4$: C, 61.34; H, 4.83; N, 13.41%. Found: C, 61.75; H, 5.01; N, 13.23%. UV-visible (DMF) λmax (nm): 267, 370. IR (KBr, cm^{-1}): 3450 ν(OH), 2929 ν(C-H str. of aliphatic -CH_2), 1698 ν(COO)asy, 1387 $\nu(COO)_{sym}$, 1613 ν(C=N), 1494 ν(N=N), 1273 ν(aromatic C-O), 1167 ν(aliphatic C-O). ^1H NMR (DMSO-*d*6, 400 MHz) δ_H: 10.33[s, 1H, Ar-OH], 8.66 [s, 1H, H-7], 8.02 [d, 1H, H-6, *J* = 2.8 Hz], 7.84 [dd, 1H, H-4, *J* = 9.2 and 2.8 Hz], 7.75 [d, 1H, H-3′], 7.60 [m, 1H, H-5′], 7.50 [m, 1H, H-4′ and H-6′], 6.78 [d, 1H, H-3, *J* = 9.2 Hz], 3.69 [m, 4H, H-8 & H-9] ppm. ^{13}C NMR (DMSO-*d*6, 100 MHz) δ_C: 174.24 [COO], 168.45 [C-7], 166.78 [C-2], 150.45 [C-1′], 141.37 [C-5], 134.29 [C-5′], 131.34 [C-2′], 129.94 [C-4′], 129.00 [C-4], 125.76 [C-6], 122.25 [C-6′], 117.58 [C-1], 115.22 [C-3], 59.65 & 55.78 [C-8 & C-9] ppm.

2.2.2. Preparation of Cyclic Dimeric Trimethyltin(IV) Complex of H_3L, $[Me_3Sn(H_2L)]_2$ (**1**)

The cyclic dimeric trimethyltin(IV) complex, $[Me_3Sn(H_2L)]_2$ (**1**) was synthesised by reacting 2-{4-hydroxy-3-[(2-hydroxyethylimino)methyl]phenylazo}benzoic acid (H_3L) with trimethyltin(IV) chloride in the stoichiometric molar ratio 1:1 (L:M) with triethylamine as a base in a refluxing condition. The ligand H_3L (0.4716 g, 1.505 mmol) in 30 mL of distilled toluene in a round bottom flask was first treated with a triethylamine base (0.1522 g, 1.505 mmol) and the mixture was then refluxed for 30 min. After that, trimethyltin(IV) chloride (0.3 g, 1.505 mmol) was added to the mixture and continually refluxed for a further 6–7 h. The reaction mixture was eventually filtered off and a yellow colored product was extracted from the solution. The product was washed thoroughly with hexane, dried and recrystallized from anhydrous toluene. The pure yellow crystals of compound **1** were finally obtained.

Yield: 0.62 g, 87.32%; m.p.: 102–103 °C. Anal.Calcd. for $C_{38}H_{46}N_6O_8Sn_2$: C, 47.93; H, 4.87; N, 8.83%. Found: C, 47.87; H, 4.50; N, 8.90%. UV-visible (DMF) λmax (nm): 268, 372. IR (KBr, cm^{-1}): 3389 ν(O-H), 2921 ν(C-H str. of Me), 1654 $\nu(COO)_{asy}$, 1493 ν(N=N), 1372 $\nu(COO)_{sym}$, 1281 ν(Aromatic C-O),1183 ν(Aliphatic C-O), 772 ν(C-H oop bending), 579 & 538 (Sn-C), 492 ν(Sn-O).^1H NMR ($CDCl_3$, 400 MHz) δ_H, Ligand skeleton: 8.48 [s, 1H, H-7], 7.91 [m, 1H, H-6], 7.70 [m, 1H, H-4], 7.63 [m, 1H, H-3′], 7.58 [m, 3H, H-4′,5′and 6′], 7.05 [d, 1H, H-3, *J* = 8.8 Hz], 4.07 [m, 1H, Aliphatic-OH], 3.98 [m, 2H, H-9, *J* = 4.4 Hz], 3.89 [m, 2H, H-8, *J* = 4.4 Hz]; Sn-CH_3 Skeleton: 0.61 [s, 9H, (Sn-CH_3)] ppm.^{13}C NMR ($CDCl_3$, 100 MHz) δ_C: Ligand skeleton: ^{13}C NMR ($CDCl_3$, 100 MHz) δ_C: 173.97 [COO], 169.32 [C-7], 151.76 [C-2], 145.70 [C-1′], 133.89 [C-5], 132.48 [C-5′], 131.14 [C-2′], 130.36 [C-4′], 128.74 [C-4], 127.75 [C-6], 119.65[C-6′], 118.13 [C-1], 117.50 [C-3]; Sn-CH_3 skeleton: −1.73 [Sn-CH_3] ppm. ^{119}Sn NMR ($CDCl_3$, 149 MHz): +139.8 ppm.

2.2.3. Preparation of Tributyltin(IV) Complex of H_3L, $Bu_3Sn(H_2L)$ (**2**)

The tri-butyltin(IV) compound (**2**) was synthesized by the reaction of the ligand, 2-{4-hydroxy-3-[(2-hydroxyethylimino)methyl]phenylazo}benzoic acid with *bis*-tributyltin

(IV) oxide by using the Dean–Stark apparatus under refluxing condition in (L:M) 1:1 molar ratio. The whole reaction was carried out in a toluene solvent as described for compound **1**. Yield: 0.26 g, 85.76%; m.p.: 86–89 °C. Anal.Calcd. for $C_{28}H_{41}N_3O_4Sn$: C, 55.83; H, 6.86; N, 6.98%. Found: C, 55.67; H, 6.85; N, 7.01%. UV-visible (DMF) λ_{max} (nm): 365, 372, 495. IR (KBr, cm^{-1}): 3450 ν(O-H), 2957 ν(C-H str. of ^{n}Bu), 1640 $\nu(COO)_{asy}$, 1494 ν(N=N), 1391 $\nu(COO)_{sym}$, 1281 ν(Aromatic C-O),1183 ν(Aliphatic C-O), 598 & 585 ν(Sn-C), 507 ν(Sn-O).^{1}H NMR ($CDCl_3$, 400 MHz) δ_H, Ligand skeleton: 8.41 [s, 1H, H-7], 7.93 [dd, 1H, H-4, J = 9.2 Hz & 2 Hz], 7.87 [s, 1H, H-6], 7.80 [d, 1H, H-3′, J = 7.2 Hz], 7.48 [s, 1H, H-5′], 7.40 [m, 1H, H-4′ and H-6′], 6.99[d, 1H, H-3, J = 9.2 Hz], 3.92 [m, 2H, H-9], 3.77 [m, 2H, H-8] ppm; Sn-^{n}Bu Skeleton: 1.65[m,6H, H-α], 1.25 [m, 12H, H-β, H-γ], 0.89 [t, 9H, H-δ] ppm. ^{13}C NMR ($CDCl_3$, 100 MHz) δ_C: 172.74 [COO-], 166.46 [C-7],151.78 [C-2], 145.04 [C-1′], 131.37 [C-5], 130.89 [C-5′], 129.77 [C-2′], 129.50 [C-4′], 129.11 [C-4], 126.50 [C-6], 118.70 [C-6′], 117.65 [C-1], 117.58 [C-3], 61.77 & 60.47 [C-8 & C-9] ppm; Sn-^{n}BuSkeleton: 27.83 [C-β] ^2J [^{119}Sn-^{13}C(19.9 Hz)], 27.07 [C-γ] ^3J [^{119}Sn-^{13}C(64.4 Hz)], 16.67 [C-α] ^1J [^{119}Sn-^{13}C(352.6 Hz)], 13.65 [C-δ] ppm. ^{119}Sn NMR ($CDCl_3$, 149 MHz): +115.97 ppm. The numbering scheme of Sn-Bu skeletal in the triorganotin complex is shown below:

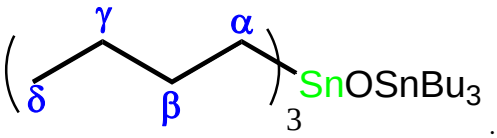

2.2.4. Preparation of Dibutyltin (IV) Complex of H_3L, $[(Bu_2Sn(H_2L))_2O]_2$ (**3**)

The dibutyltin(IV) complex $[(Bu_2Sn(H_2L))_2O]_2$ (**3**) was synthesized in a toluene solvent by the reaction of the ligand 2-{4-hydroxy-3-[(2-hydroxyethylimino)methyl]phenylazo}benzoic acid with dibutlytin(IV) oxide with the use of Dean-Stark apparatus under refluxing condition at 1:1 (L:M) stoichiometric ratio. Yield: 0.50 g, 74.86%; m.p.: 201–203 °C. Anal.Calcd. for $C_{96}H_{132}N_{12}O_{18}Sn_4$: C, 52.01; H, 6.00; N, 7.58%. Found: C, 51.65; H, 5.61; N, 7.13%. UV-visible (DMF) λ_{max} (nm): 265, 273, 483. IR (KBr, cm^{-1}): 3442 ν(O-H), 2957 ν(C-H str. of ^{n}Bu), 1630 $\nu(COO)_{asy}$, 1470 ν(N=N), 1394 $\nu(COO)_{sym}$, 1311 ν(Aromatic C-O),1193 ν(Aliphatic C-O), 595 & 581 ν(Sn-C), 538 ν(Sn-O). ^{1}H NMR ($CDCl_3$, 400 MHz) δ_H, Ligand skeleton: 9.91 [s, 1H, H-7], 8.31 [dd, 1H, H-6], 8.19 [m, 1H, H-4], 7.85 [m, 1H, H-3′], 7.54 [m, 1H, H-5′], 7.06 [m, H-4′ and H-6′], 6.95 [m, 1H, H-3], 4.07 [m, 1H, aliphatic-OH], 3.83 [m, 4H, H-8 & H-9] ppm; Sn-^{n}Bu Skeleton: 1.46 [m,12H, H-α, H-β, H-γ], 0.91 [m, 6H, H-δ] ppm. ^{13}C NMR ($CDCl_3$, 100 MHz) δ_C: 171.76 [COO-], 167.23 [C-7],150.51 [C-2], 147.23 [C-1′ and C-9], 133.79 [C-5 and C-8], 131.40 [C-5′], 129.74 [C-2′], 128.89 [C-4′], 128.07 [C-4], 125.75 [C-6], 119.63 [C-6′], 117.45 [C-1], 116.06 [C-3]; Sn-^{n}Bu Skeleton: 29.70[C-β], 27.29 [C-γ], 26.47 [C-α], 13.58 [C-δ] ppm. ^{119}Sn NMR ($CDCl_3$, 149 MHz): −93.1 and −140.4 ppm. The numbering scheme of Sn-Bu skeletal in the diorganotin complex is shown below:

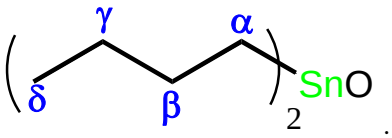

2.3. Crystallographic Data Collection and Structure Refinement

Single crystal X-ray diffraction data were collected using the ω-scan technique using MoKα (λ = 0.71073Å) radiation. The title compound was studied at 100 K using a RIGAKU XtaLAB Synergy, Dualflex, Pilatus 300 K diffractometer [32] with Photon Jet micro-focus X-ray Source. Data collection, cell refinement, data reduction and absorption correction were carried out using CrysAlis PRO software [32]. The crystal structures were solved by using direct methods with the SHELXT 2018/3 program [33]. Atomic scattering factors were taken from the International Tables for X-ray Crystallography. Positional parameters of non-H-atoms were refined by a full-matrix least-squares method on F2 with anisotropic thermal parameters by using the SHELXL 2018/3 program [34]. Hydrogen atoms participating in hydrogen bonding were found on the Fourier map and freely refined while the others were

placed in calculated positions (C–H = 0.93–0.98 Å) and included as riding contributions with isotropic displacement parameters set to 1.2-times the Ueq of the parent atom. Crystal data and structure refinement parameters are shown in Table 1.

Table 1. Crystal data and structure refinement parameters for complex **1**.

Parameters	1
Empirical formula	$C_{38}H_{46}N_6O_8Sn_2$
Formula weight	952.23
Temperature (K)	100 (3)
Wavelength (Å)	0.71073
Crystal system	triclinic
Space group	P-1
a (Å)	7.1138 (1)
b (Å)	10.4253 (2)
c (Å)	14.0461 (2)
α (°)	94.753 (1)
β (°)	93.448 (1)
γ (°)	108.603 (1)
Volume ($Å^3$)	979.74 (3)
Z	1
Density (Mg/m^3)	1.614
Absorp. coeff. (mm^{-1})	1.333
F (000)	480
Crystal size (mm^3)	0.04 × 0.05 × 0.33
Theta range for data collection	2.9, 25.0
Index ranges	−8<= h <=8; −12<= k <=12; −16<= l <=16
Reflection collected	26,309
Data completeness	99.9%
Independent reflections	3559 [R(int) = 0.022]
Goodness of fit on F^2	1.11
Final R indices [I > 2sigma(I)]	0.0152
R indices (all data)	0.0159
Largest diff. peak and hole (e $Å^{-3}$)	0.58 and −0.22

2.4. Computational Details

The Hirshfeld molecular surface was generated by the CrystalExplorer program (version 17.5) [35,36]. The normalized contact distances, d_{norm} [37], based on Bondi's van der Waals radii [38], were mapped into the Hirshfeld surface. The DFT calculations based on the experimental X-ray geometry of **1** were carried out using the dispersion-corrected hybrid functional ωB97XD [39] with the help of Gaussian-09 [40] program package. The Douglas–Kroll–Hess 2nd order scalar relativistic calculations requesting relativistic core Hamiltonian were carried out using the DZP-DKH basis sets [41–44] for all atoms. The topological analysis of the electron density distribution with the help of the quantum theory of atoms-in-molecules (QTAIM) method, electron localization function (ELF), and reduced density gradient (RDG) analyses were performed using the Multiwfn program (version 3.7) [45].

2.5. Antibacterial Studies

The antibiotic activities of the ligand (**H_3L**) and the compounds (**1**–**3**) were studied against the three gram-negative bacterial strains viz. *Klebsiella pneumoniae* (A), *Vibrio cholera* (M), *Shigella boydii* (Q) andtwo gram-positive bacterial strains *viz. Staphylococcus aureus* (J) and *Streptococcus pneumonia* (K) according to the Kirby–Bauer Disk Diffusion Susceptibility Test Protocol [46]. The standard antibiotics such as Polymyxin B and Gentamycin were used as positive control against gram-negative bacteria and Vancomycin for gram-positive bacteria. They were treated at various concentrations. In order to determine the zone of inhibition, discs of 5 mm in diameter were used on pre-spread bacterial strains in a nutrient

agar plate. Strains were treated with the compounds at different concentrations (1 µg/disc, 100 µg/disc and 500 µg/disc). After 18–24 h of incubation at 37 °C, the diameters (mm) of clear zone of inhibitions were measured using a scale.

3. Results and Discussion

3.1. Synthesis

The ligand, an azo-imine carboxylate Schiff base, was synthesized by condensation of 2-(3-formyl-4-hydroxyphenylazo) benzoic [30] with ethanolamine in toluene at warm condition. The newly obtained ligand, 2-{4-hydroxy-3-[(2-hydroxyethylimino)methyl]phenylazo}benzoic acid (**H_3L**) was subjected to develop Sn(IV) compounds. Thus, the three new organotin(IV) complexes (**1–3**) were synthesized by the reaction of **H_3L** with appropriate alkyl tin(IV) precursors such as: trimethyltin(IV) chloride, *bis*-tributyltin(IV) oxide and dibutyltin(IV) oxide in refluxing condition by the use of distilled toluene. The single crystals of the complex **1** were obtained from the reaction mixture, whereas the complexes **2** and **3** were recrystallized from toluene. The three complexes were obtained in good yield and all the three complexes **1–3** were found to be soluble in all common organic solvents. The reaction scheme for the synthesis of the complexes **1–3** is shown in Scheme 1.

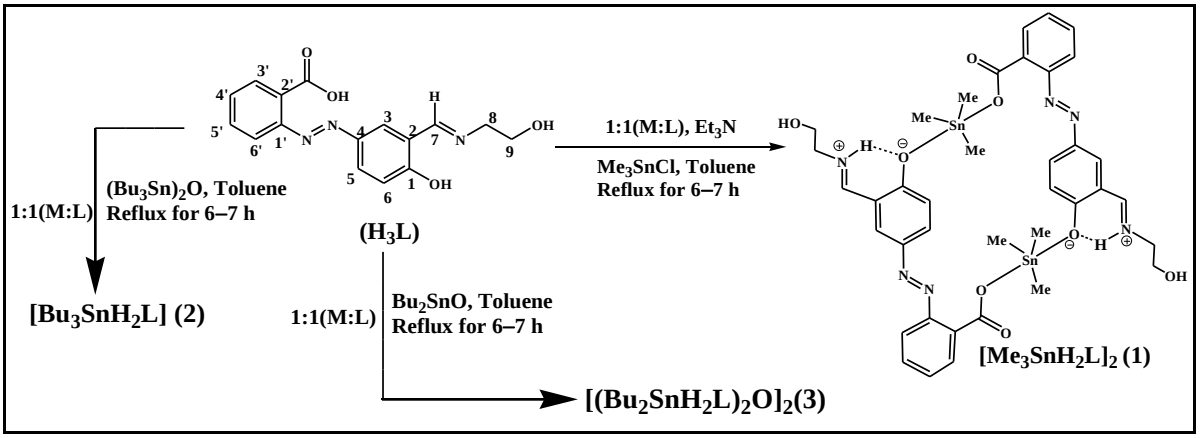

Scheme 1. The reaction scheme for the synthesis of complexes **1**, **2** and **3**.

3.2. IR-Spectroscopy

The IR spectroscopic data for the ligand (**H_3L**) and the complexes (**1–3)** are given in the Experimental section, and their spectra are shown in Figures S1–S4 (see Supplementary Materials). The ligand has various functional groups such as carboxylate, aliphatic and phenolic-OH, carbonyl (-C=O), azo (-N=N-), imine (-C=N-), aromatic -C=C-, aliphatic and aromatic-C-O. These appeared in the spectra in the usual positions for the ligand and its Sn(IV) complexes. The overlapping stretching frequencies of all the –OH groups appear as strong and broad band at 3450 cm^{-1} in H_3L. The band is quite sharp and shifts to lower frequency at 3389 cm^{-1}, indicating involvement of carboxylate-O and phenolic-O coordination to Sn(IV) in the complex **1**. However, there is not much change observed in complexes **2** and **3**. The weak band for aliphatic –CH_2- groups can be seen at 2929 cm^{-1} for H_3L and at 2921 cm^{-1} for the complex **1**. However, in complexes **2** and **3**, it is very prominent and multiplet in form, indicating coordination of the ligand to Sn(IV) that has a butyl substituent. The asymmetric ($\nu_{(COO)asy}$) and symmetric ($\nu_{(COO)sy}$) stretching frequencies of the carboxylate group in the ligand appear at 1698 cm^{-1} and 1385 cm^{-1}, respectively. As a result of COO-coordination to Sn(IV), these bands shift to the frequency range at 1630–1654 cm^{-1} for asymmetric -COO and 1372–1394 cm^{-1} for symmetric-COO [10,15–17,21,30]. The difference between the asymmetric and symmetric frequencies, i.e., $\Delta\nu(_{\nu(COO)asy} - \nu_{(COO)sym})$ is 282, 248 and 236 cm^{-1} respectively for the complexes **1**, **2** and **3**, which are greater than 200 cm^{-1}, indicating that the carboxylate group coordinates to Sn(IV) in monodentate mode in each complex [15,16]. The -C=N-, -C=C-, and -N=N- bands appear in the

usual positions in the spectra of the ligand and the complexes, respectively ranging from 1645–1494 cm^{-1} (**H_3L**), 1615–1493 cm^{-1} (**1**), 1620–1472 cm^{-1} (**2**), and 1610–1470 cm^{-1} (**3**). The bands for aromatic and aliphatic-C-O groups can be seen at 1273 and 1167 cm^{-1} for **H_3L**, 1281 and 1183 cm^{-1} for **1**, **2**, and 1311 and 1193 for **3** cm^{-1}, respectively. All the compounds exhibit a strong band for out-of-plane bending of ring C-H bonds in the range of 750 (complex **3**) to 772 (complex **1**). The Sn-C band of the complex **1** is doublet in nature (579 and 538 cm^{-1}), which means that the Sn-C bonds are non-linear and the Sn-O bond is sharp at 492 cm^{-1}. For complexes **2** and **3**, these are assigned in a similar way (for **2**: 598, 585 cm^{-1} and 507 cm^{-1}; for **3**: 595, 581 cm^{-1} and 538 cm^{-1}) to Sn-C and Sn-O bonds, respectively [10,21,30].

3.3. Multinuclear (^{1}H, ^{13}C and ^{119}Sn) NMR-Spectroscopy

The NMR spectra of the ligand (**H_3L**) were recorded in DMSO-d_6 solvent, whilst these were recorded in the $CDCl_3$ solvent for the complexes **1–3**; their spectral data are provided in the experimental section. The ^{1}H NMR spectra of the ligand and the complex **1** are given in Figures 1 and 2; all other spectra including ^{1}H NMR and ^{13}C NMR are placed in Figures S5–S10 (Supplementary Materials). While the aromatic protons of the azo-imino ligand **H_3L** are seen in the range of 6.78–8.02 ppm (Figure 1), the aromatic protons in all the complexes **1–3** are found to be in the range of 6.94–8.43 ppm. The imine protons of all the compounds are found at 8.67 ppm for **H_3L** and at 8.48, 8.41 and 9.91 ppm, respectively, for **1–3** compounds. The phenolic-OH at 10.33 ppm for the ligand is virtually absent in the complexes. The carboxylate-OH, which is absent in the ligand spectra due to the DMSO solvent, is absent in complexes **1** and **3**, but present in complex **2** spectra. For the ligand **H_3L**, the four methylene protons attached with imino/OH functions appear as a triplet at 3.69 ppm, while the same protons appear in the range of 4.11–3.76 ppm for the three complexes **1–3**. Based on the Sn-alkyl protons signals, the complexes could be distinguished from the uncoordinated ligand, as well as from one another. The complex **1** has Sn-methyl groups, which is detected as a singlet peak at 0.61 ppm [21]; the complex **2** has Sn-Bu_3, which results in two distinct peaks as a triplet peak at 0.89 ppm and two multiplets in the range of 1.25–1.66 ppm for the methyl and the three methylene protons, respectively; similarly, the complex **3** with Sn-Bu_2 shows two multiplet peaks in the range of 0.91–1.46 ppm for tin-butyl protons [10,21].

The ^{13}C-NMR spectrum of the azo-imino carboxylate ligand **H_3L** is shown as a δ(COO) signal at 174.25 ppm, whereas the signal in the spectra of complexes is shifted downfield and appears at 173.97, 172.74, and 171.76 ppm for **1**–**3**, respectively. The imine carbons can be found at 168.46 (**H_3L**), 169.32 (**1**), 166.46 (**2**), and 167.24 (**3**) ppm. The aromatic ring carbons of the ligand **H_3L** show signals in the range of 166.79–115.22 ppm (Figure S7), but the same signals are found in the range of 116.07–151.78 ppm in the spectra of the complexes **1–3** (Figures S8–S10). In the ligand spectrum, the ethylene carbons are found at 59.66 and 55.79 ppm, and in the complex **2** it is at 61.77 and 60.47 ppm. In complex **1**, the tin-methyl-carbon shows a highly shielded signal at −1.73 ppm. Moreover, the complexes **2** and **3** have tin-butyl carbons (c-α, c-β, c-γ, c-δ), which appear in the range of 27.93–13.65 ppm for **2** and of 31.93–13.58 ppm for **3**.

Moreover, the geometry and coordination number of the complex **2** can be predicted from its carbon satellites (Figure S9) by determining ^nJ (^{119}Sn-^{13}C) coupling constant values [15,16,21]. The complex **2** has 352.6 Hz, 19.9 Hz and 64.4 Hz coupling constant for ^1J (^{119}Sn-^{13}C), ^2J (^{119}Sn-^{13}C) and ^3J (^{119}Sn-^{13}C) coupling satellites, respectively, indicating that the complex has four coordinate quasi tetrahedral geometry around tin centres [15,16,21] in the solution state. It was further confirmed by its ^{119}Sn NMR spectral signal [15], which is found at +115.98 ppm (Figure 3). The ^{119}Sn NMR spectral signal at +139.86 ppm (Figure 3) for the complex **1** also reveals that it has a similar structure in the solution to complex **2**, whereas in the case of complex **3,** two sharp signals of ^{119}Sn NMR spectrum are found at −93.1 and −140.4 ppm, which indicate that it must have two types of tin centres with a distorted trigonal bipyramidal geometry [10].

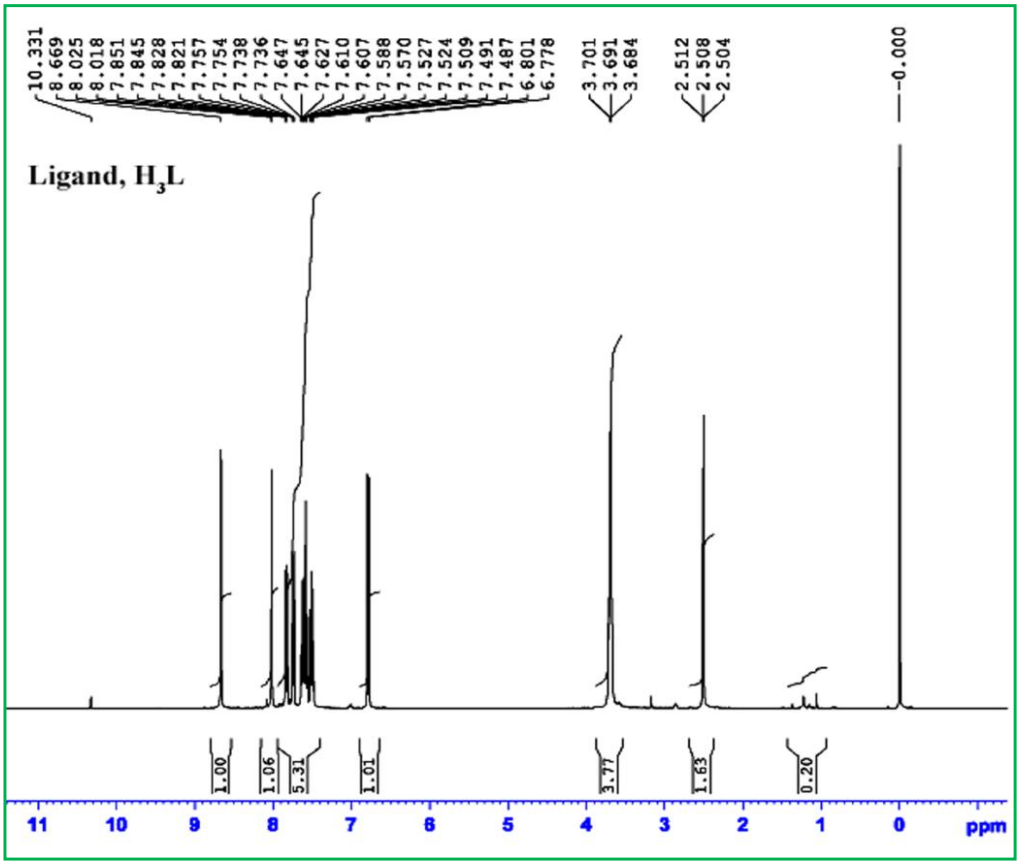

Figure 1. ^{1}H NMR spectrum of the Ligand, H_3L.

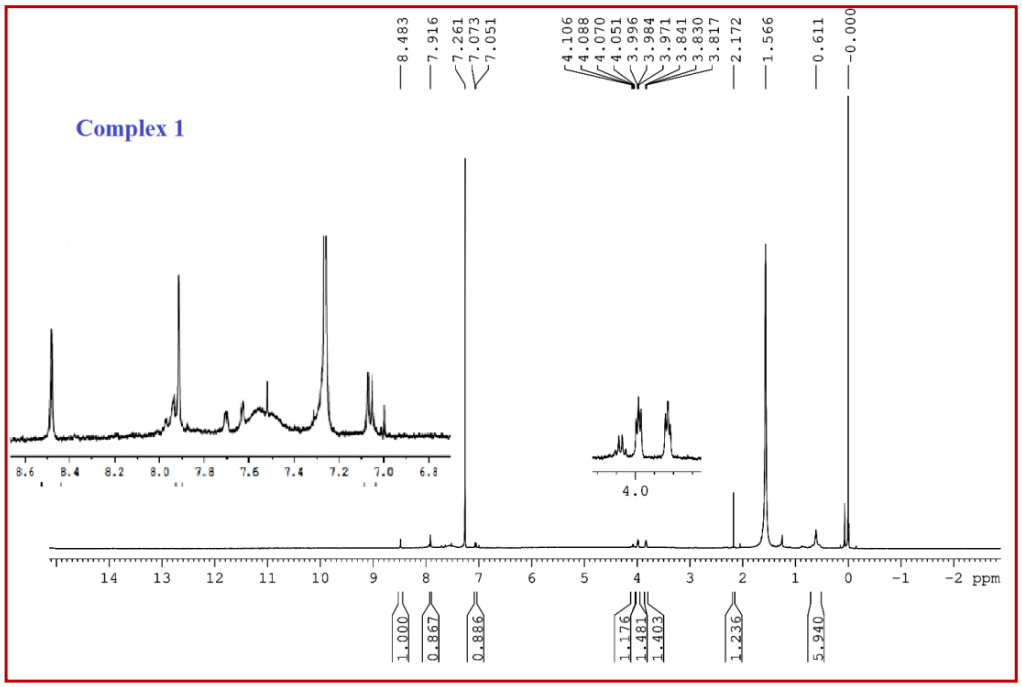

Figure 2. ^{1}H NMR spectrum of the complex **1**.

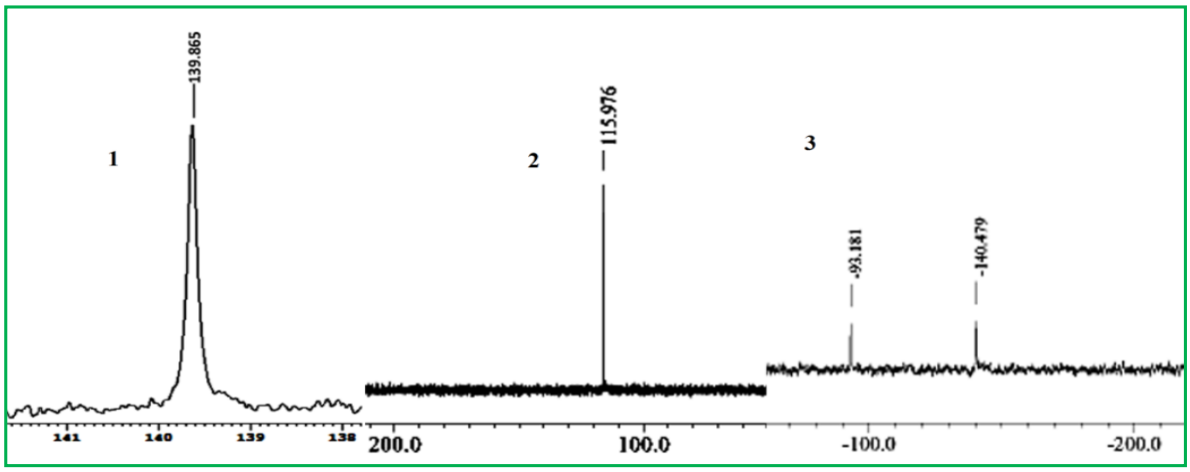

Figure 3. ^{119}Sn NMR spectra of the complexes **1**, **2** and **3**.

3.4. Crystal Structure of **1**

The ORTEP view with atom numbering of the complex **1** is shown in Figure 4. It is a cyclic dimer of triorganotin(IV) ($C_{38}H_{46}N_6O_8Sn_2$) with the asymmetric unit $Me3Sn^{IV}(H_2L)$. It is a triclinic crystal system with the space group P-1. The coordination environment about Sn(IV) is trigonal-bipyramidal, constituted by the three methyl group at the equatorial positions and the two axial positions occupied by the one carboxylate group via unidentate fashion and one phenoxo group from the ligand moiety. The coordinate ligand is in the zwitterionic state, where phenolic H-atom shifts to the imino-N atom, forming a 6-membered ring through H-bonding. The distortion of coordination sphere of Sn(IV) can be characterized quantitatively by parameter τ, defined by Addison et al. [47] (the τ values for the idealized geometries are τ = 0, square planar, τ = 1, trigonal bipyramidal). The value of τ = (b − a)/60 where b is the largest and a is the second largest basal angle around the tin atom] for complex **1** is 0.94. The selected bond lengths, bond angles and hydrogen bonds geometry are presented in Tables 2 and 3, respectively. The coordinated ligand is in azo-form with N1-N2 bond length of 1.261(2) Å, which is comparable with literature [21,25,30].

Table 2. The selected bond lengths (Å) and bond angles (°) for **1**.

Atoms	Bond Length (Å)
Sn1-O1	2.2126 (11)
Sn1-C1	2.1270 (18)
Sn1-C2	2.1306 (15)
Sn1-C3	2.1303 (19)
Sn1-O3 ^{i}	2.3091 (11)
N1-N2	1.261 (2)
Atoms	**Bond Angle (°)**
O1-Sn1-C1	95.52 (6)
O1-Sn1-C2	93.02 (6)
O1-Sn1-C3	86.09 (6)
O1-Sn1-O3 ^{i}	177.68 (5)
C1-Sn1-C2	117.20 (7)
C1-Sn1-C3	121.47 (8)
O3 ^{i}-Sn1-C1	84.61 (5)
C2-Sn1-C3	121.13 (7)
O3 ^{i}-Sn1-C2	88.97 (6)
O3 ^{i}-Sn1-C3	91.86 (6)

Symmetrycode: ^{i} 1 − x, 2 − y, 1 − z.

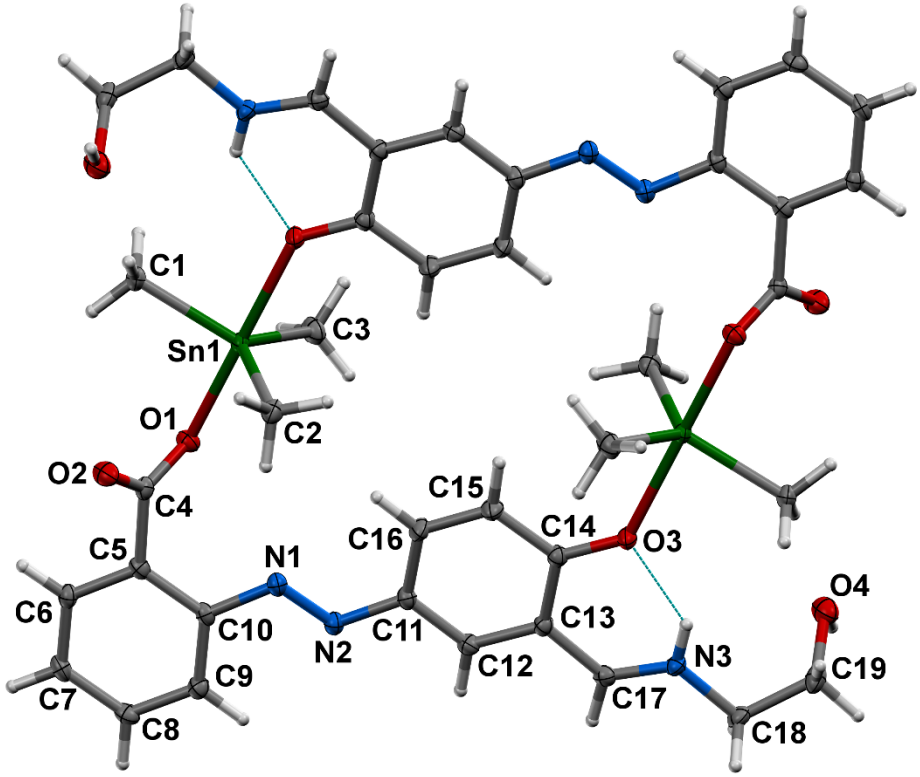

Figure 4. The crystal structure of the complex **1**. Displacement ellipsoids are drawn at 50% probability level.

Table 3. The hydrogen bonding parameters for compound **1**.

Compound	D–H ... A	d (D–H)	d (H ... A)	d (D ... A)	<(DHA)
1	N3-H3 ... O3	0.83 (2)	1.97 (2)	2.6316 (18)	136 (2)
	O4-H4 ... O2 [ii]	0.85 (3)	1.96 (3)	2.7829 (18)	159 (3)
	C18-H18B ... O2 [iii]	0.99	2.56	3.529(2)	167

Symmetrycode: [ii] x, y, 1 + z [iii] −x, 1 − y, 1 − z.

The imine bond length (N3-C17 of 1.293(2) Å) is also comparable with the literature value [21,22,30]. The complex is viewed as end-to-end bridged by the ligand, OOC-H_2L-O to Me_3Sn^{IV} fragment. The C-Sn-C angles are of 117.20(7), 121.47(8), and 121.13(7)° and the O-Sn-O angle is 177.68(5)°. The Sn-C bonds are almost equivalent (Sn1-C1, 2.1270(18) Å; Sn1-C2, 2.1306(15) Å Sn1-C3, 2.1303(19) Å). In the case of Sn-O bonds, the Sn1-O1(carboxylate-O) (2.2126(11) Å) is shorter than that of Sn1-O3(phenolate-O) (2.3091(11) Å). Thus, the complex possesses somewhat distorted trigonal bipyramidal geometry about Sn(IV), where axial bonds are longer than the equatorial bonds. The distance between Sn1 and other carboxylate oxygen is 3.303 Å, which is in line with the sum of their Van der Waals radii. Thus, it can be treated as a strong secondary interaction. The complex has a centre of symmetry with plane-centroid-Sn distance, 4.00 Å. The complex holds an intramolecular and an intermolecular H-bonding between N3-H3 ... O3 and O4-H4 ... .O2 [i] ([i] +x, 1 + y, 1 + z), respectively (Table 3, Figure S11). Another similar type, but with longer H-bonding, occurs between C18-H18B ... .O2 [ii] ([ii] −x, 1 − y, 1 − z).

3.5. Theoretical Study of Intermolecular Interactions

The molecular Hirshfeld surface (visualization of short interatomic contacts using sums of appropriate vdW radii) represents an area where molecules come into contact, and its analysis gives the possibility of an additional insight into the nature of intermolecular interactions in the crystal state. We carried out the Hirshfeld surface analysis for the X-ray structure of **1** to understand what kind of intermolecular contacts gives the largest

contributions in crystal packing (Figure 5). For the visualization, we have used a mapping of the normalized contact distance (d_{norm}); its negative value enables identification of molecular regions of substantial importance for the detection of short contacts. In the Hirshfeld surface, the regions of shortest intermolecular contacts are visualized by red circle areas (corresponding to hydrogen bonds O–H···O and stacking interactions). The fingerprint plots from the Hirshfeld surface analysis for the X-ray structure of **1** are given in Figure S12. Results of the Hirshfeld surface analysis for the X-ray structure of **1** reveal that intermolecular contacts involving hydrogen atoms (viz. H···H, O···H, and C···H) give the largest contributions in the crystal packing.

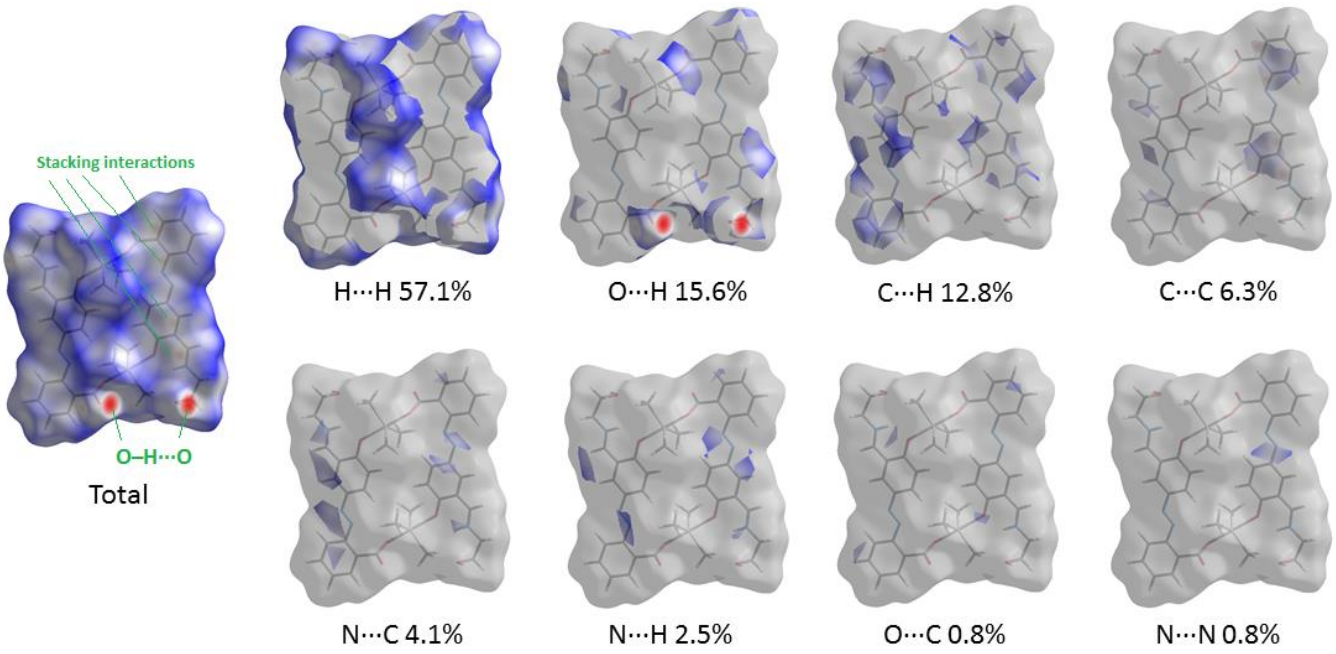

Figure 5. Results of a Hirshfeld surface analysis for the X-ray structure **1**.

We carried out DFT calculations, followed by the topological analysis of the electron density distribution, at the ωB97XD/DZP-DKH level of theory for model supramolecular associates to more deeply study the phenomenon of hydrogen bonds O–H···O and stacking interactions in the X-ray structure of **1**. Results of topological analysis of the electron density distribution are summarized in Table 4; the contour line diagrams of the Laplacian of electron density distribution $\nabla^2\rho(\mathbf{r})$, visualization of electron localization function (ELF) and reduced density gradient (RDG) analyses for hydrogen bonds O–H···O and stacking interactions in the X-ray structure of **1** are shown in Figure 6.

Table 4. Values of the density of all electrons—$\rho(\mathbf{r})$, Laplacian of electron density—$\nabla^2\rho(\mathbf{r})$ and appropriate λ_2 eigenvalues, energy density—H_b, potential energy density—$V(\mathbf{r})$, Lagrangiankinetic energy—$G(\mathbf{r})$, and electron localization function—ELF (a.u.) at the bond critical points (3, −1), corresponding to hydrogen bonds O–H···O and stacking interactions in the X-ray structure of **1**, and estimated strength for these contacts E_{int} (kcal/mol).

Contact	$\rho(\mathbf{r})$	$\nabla^2\rho(\mathbf{r})$	λ_2	H_b	$V(\mathbf{r})$	$G(\mathbf{r})$	ELF	E_{int} *
O–H···O 1.958 Å	0.024	0.094	−0.024	0.003	−0.018	0.021	0.067	5.6
C···C 3.310 Å	0.006	0.019	−0.006	0.001	−0.003	0.004	0.022	0.9

* $E_{int} \approx -V(\mathbf{r})/2$.

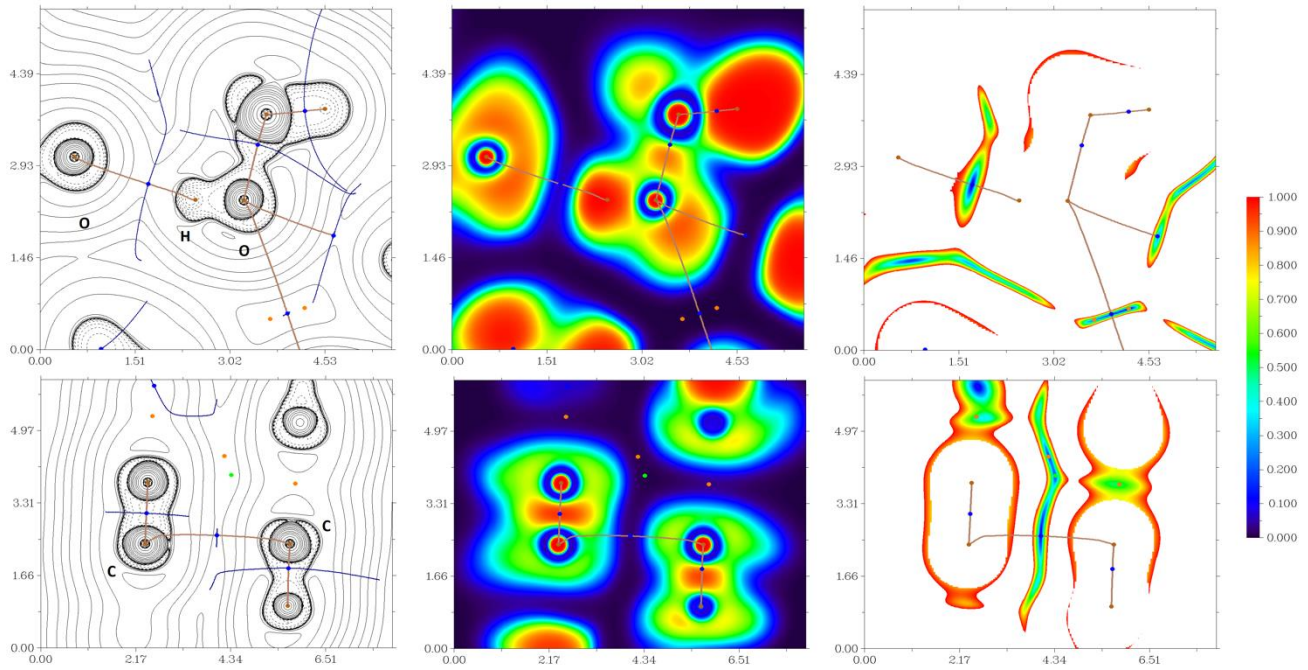

Figure 6. Contour line diagrams of the Laplacian of electron density distribution $\nabla^2\rho(\mathbf{r})$ and selected zero-flux surfaces (left panels), visualization of electron localization function (ELF, center panels) and reduced density gradient (RDG, right panels) analyses for hydrogen bond O–H···O (top) and stacking interactions (bottom) in the X-ray structure of **1**. Bond critical points (3, −1) are shown in blue, nuclear critical points (3, −3)—in pale brown, ring critical points (3, +1)—in orange, cage critical points (3, +3)—in light green, length units—Å, and the color scale for the ELF and RDG maps is presented in a.u.

The topological analysis of the electron density distribution in model supramolecular associates demonstrates the presence of bond critical points (3, −1) for hydrogen bonds O–H···O and stacking interactions in the X-ray structure of **1** (Table 4 and Figure 6). The low magnitude of the electron density, positive values of the Laplacian of electron density, and very close to zero positive energy density in these bond critical points (3, −1) and estimated strength for appropriate short contacts are typical for weak noncovalent interactions. The balance between the Lagrangian kinetic energy G(**r**) and potential energy density V(**r**) at the bond critical points (3, −1) for hydrogen bonds O–H···O and stacking interactions in the X-ray structure of **1** (viz. $-G(\mathbf{r})/V(\mathbf{r}) > 1$) reveals that covalent contribution in these short contacts is negligible [48]. The Laplacian of electron density is typically decomposed into the sum of contributions along the three principal axes of maximal variation, giving the three eigenvalues of the Hessian matrix (λ_1, λ_2 and λ_3), and the sign of λ_2 can be utilized to distinguish bonding (attractive, $\lambda_2 < 0$) weak interactions from nonbonding ones (repulsive, $\lambda_2 > 0$) [49,50]. Thus, hydrogen bonds O–H···O and stacking interactions in the X-ray structure of **1** are attractive. Note that estimated cumulative strengths of hydrogen bonds O–H···O and stacking interactions responsible for the formation of formal dimers in the X-ray structure of **1** by conventional supermolecule method (as the difference between the total electronic energies of appropriate dimer and two monomers) are 44.8 and 46.3 kcal/mol, respectively.

3.6. Antibacterial Activities

Antibacterial activities of the ligand (**H_3L**) and the compounds (**1**–**3**) were evaluated at different concentrations (1 μg/disc, 100 μg/disc, 500 μg/disc) and compared with the standard antibiotics. The *Klebsiella pneumoniae* (A), *Vibrio cholerae* (M) and *Shigella boydii* (Q) (gram-negative) and *Staphylococcus aureus* (J), *Streptococcus pneumonia* (K) (gram-positive) bacteria were included as bacterial strains. The *Polymyxin B* and Gentamicin as standard

antibiotics against gram-negative bacteria and *Vancomycin* against gram-positive bacterial strains were used as positive control at four different concentrations (10 µg/disc, 30 µg/disc, 100 µg/disc, 500 µg/disc) in order to compare with the activity of the tested compounds. The calculated zones of inhibitions were measured and the data are given in Table 5. The data are represented in bar-diagram in Figure 7 for the ligand and Figure 8 for the complex **1**. The zone diameter is the measure of activity; the zone diameter activity is higher and stronger. The *Vancomycin*, an antibiotic drug for gram (+) bacteria only, shows lethal activity at 30 µg/disc concentration against gram-positive bacterial strains *viz. Staphylococcus aureus* (J) (Zone diameter, 14 ± 0 mm), *Streptococcus pneumonia* (K) (Zone diameter, 12 ± 0 mm) and remains inactive at higher concentrations (100 µg/disc and 500 µg/disc). The activities of the compounds are less or comparable (see Table 5) with the standard drug. Most importantly, they show activity even at a lower concentration—1 µg/disc (e.g., 6.3 ± 0.5 and 10.7 ± 0.5 for **3**)—and increases with an increase in concentrations. Their activities are more or less the same. On the other hand, the standard gram (−) ve antibiotic drugs, *Polymyxin B* for *Klebsiella pneumoniae* (A) and Gentamicin for *Vibrio cholerae* (M) and *Shigella boydii* (Q) bacteria show lethal activity at concentrations 10 µg/disc, 100 µg/disc and 500 µg/disc but not at 30 µg/disc (see Table 5). However, the compounds ($\mathbf{H_3L}$ and complexes, **1–3**) under investigation show lethal activity against all kinds of bacterial strains at all concentrations. The *Polymyxin B* show zone of inhibition ranges from 5.0 ± 0.0 to 12.0 ± 0.6 mm against *Klebsiella pneumoniae* (A), which is exclusively comparable with the compounds ($\mathbf{H_3L}$: 6.0 ± 1.0–14.0 ± 1.0; **1**: 5.0 ± 0.0–13.7 ± 0.6 mm). The activities of Gentamicin range from 15 ± 0.0–25 ± 0.0 against *Vibrio cholerae* (M) and 17.0 ± 0.6–36.7 ± 0.6 against *Shigella boydii* (Q) bacteria. The activities of the compounds against these bacteria are less or comparable (e.g., $\mathbf{H_3L}$: 5.0 ± 0.0–13.7 ± 0.6 against *Vibrio cholerae* (M) and 5.7 ± 1.0–15.3 ± 1.0 against *Shigella boydii* (Q); **2**: 8.3 ± 1.0–18.7 ± 1.0 against *Vibrio cholerae* (M) and 6.3 ± 1.0–18.0 ± 0.0 against *Shigella boydii* (Q)). The study highlights two important characteristic points regarding their potential antibacterial properties; first, they are active evenly against both types of bacteria; second, their activities are comparable against the corresponding standard drugs. Thus, the compounds could be treated as common potential antibacterial materials.

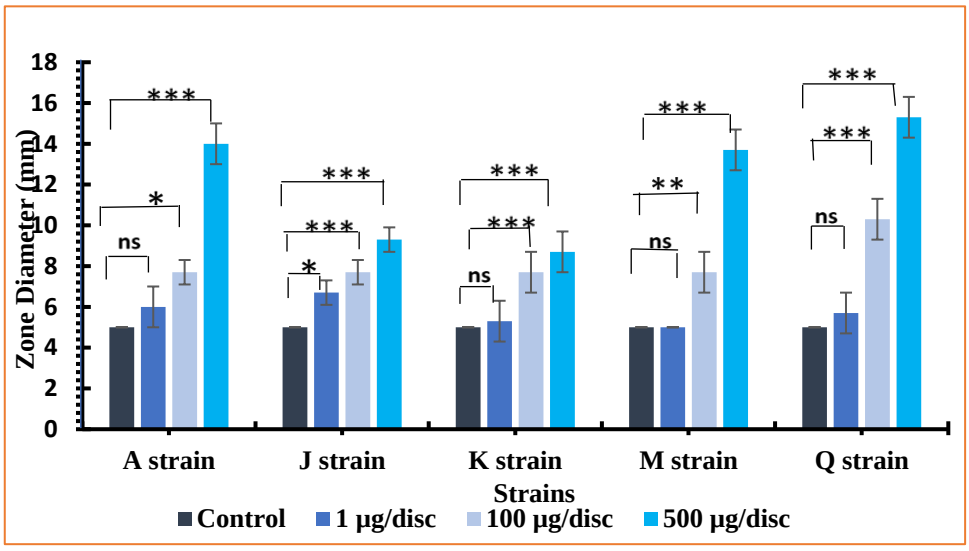

Figure 7. The zone diameter at different concentrations of $\mathbf{H_3L}$ on Strains, *Klebsiellapneumoniae* (A), *Staphylococcus aureus* (J), Streptococcus *pneumonia* (K), *Vibrio cholerae* (M) & *Shigella boydii* (Q). Data are represented as mean ± SD of three concentration of doses (* $p < 0.05$, ** $p < 0.01$, *** $p < 0.001$, ns—no significance $p > 0.05$).

Table 5. Antibacterial activities of the compounds and standard drugs against three (−) ve and two (+) ve bacteria.

Compounds	Conc.	Zone of Inhibition at Different Concentration (mm)				
		Gram (−) ve Bacteria			Gram (+) ve Bacteria	
		K. pneumoniae (A)	*V. cholerae* (M)	*Shigella boydii* (Q)	*S. Aureus* (J)	*S. Pneumoniae* (K)
Control		5.0 ± 0.00	5.0 ± 0.00	5.0 ± 0.00	5.0 ± 0.00	5.0 ± 0.00
Polymyxin B	10 µg	5.0 ± 0.0	-	-	-	-
	100 µg	7.0 ± 0.0	-	-	-	-
	500 µg	12.0 ± 0.6	-	-	-	-
Gentamicin	10 µg	-	15 ± 0.0	17 ± 0	-	-
	100 µg	-	22 ± 0.0	23.3 ± 0.6	-	-
	500 µg	-	25 ± 0.0	36.7 ± 0.6	-	-
Vancomycin	30 µg	-	-	-	14 ± 0	12 ± 0
H_3L	1 µg	6.0 ± 1.0	5.0 ± 0.0	5.7 ± 1.0	6.7 ± 0.6	5.3 ± 1.0
	100 µg	7.7 ± 0.6	7.7 ± 1.0	10.3 ± 1.0	7.7 ± 0.6	7.7 ± 1.0
	500 µg	14.0 ± 1.0	13.7 ± 1.0	15.3 ± 1.0	9.3 ± 0.6	8.7 ± 1.0
1	1 µg	5.0 ± 0.0	5.0 ± 0.0	5.0 ± 0.0	6.0 ± 0.0	6.0 ± 0.0
	100 µg	6.7 ± 0.6	9.0 ± 0.0	11.7 ± 1.0	7.3 ± 0.6	8.7 ± 0.6
	500 µg	13.7 ± 0.6	13.7 ± 1.0	5.0 ± 0.0	10.3 ± 0.6	14.7 ± 0.6
2	1 µg	5.0 ± 0.0	8.3 ± 1.0	6.3 ± 1.0	6.3 ± 0.6	6.0 ± 0.0
	100 µg	5.0 ± 0.0	17.7 ± 1.0	14.7 ± 1.0	7.0 ± 0.0	7.3 ± 0.6
	500 µg	6.3 ± 0.6	18.7 ± 1.0	18.0 ± 0.0	8.7 ± 0.6	8.0 ± 1.0
3	1 µg	5.0 ± 0.0	5.0 ± 0.0	6.0 ± 0.0	6.3 ± 0.5	10.7 ± 0.5
	100 µg	5.0 ± 0.0	11.7 ± 0.5	14.7 ± 0.5	7.0 ± 0.0	6.0 ± 0.0
	500 µg	5.0 ± 0.0	8.3 ± 0.5	19.7 ± 0.5	8.7 ± 0.5	9.3 ± 0.5

'-' means no activity; Polymyxin B and Gentamicin shows no activity at conc. 30 µg but Vancomycin only at conc. 30 µg.

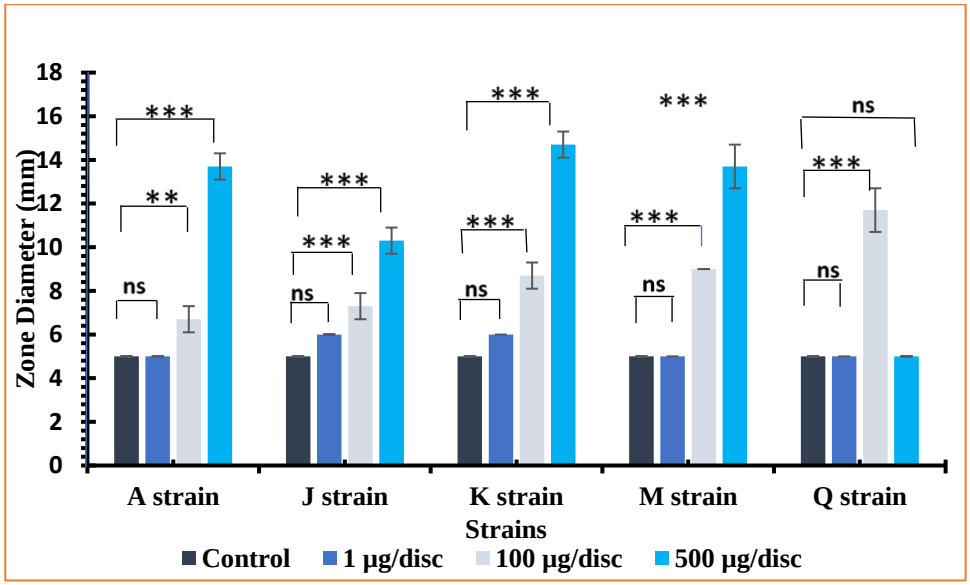

Figure 8. The zone diameter at different concentrations of complex (**1**) on Strains *Klebsiella pneumoniae* (**A**), *Staphylococcus aureus* (**J**), *Streptococcus pneumoniae* (**K**), *Vibrio cholerae* (**M**) & *Shigella boydii* (**Q**). Data are represented as mean ± SD of three concentration of doses (** $p < 0.01$, *** $p < 0.001$, ns—no significance $p > 0.05$).

4. Conclusions

A new ligand containing versatile functional groups, including azo-, imine-, phenolic-OH, alcoholic-OH and carboxylate functions, was synthesized. The ligand generates versatile organotin(IV) complexes. With trimethyltin(IV), the ligand forms a 24-membered cyclic dimeric organotin(IV) complex. In the solid state, various noncovalent interactions, including stacking and hydrogen bonding, determine molecular packing. The solid state TBP geometry about Sn(IV) changes into a distorted tetrahedral geometry in the solution. Again, with tributyltin(IV), the ligand forms distorted tetrahedral geometry in the solution, but with dibutyltin(IV), the ligand shows distorted trigonal bipyramidal geometry with a two tin centre. The compounds possess considerable antibacterial activity against both gram-negative and gram-positive bacteria. Thus, the compounds can be an effective potential common antibacterial material.

Supplementary Materials: The following supporting information can be downloaded at: https://www.mdpi.com/article/10.3390/cryst12111582/s1, Supplementary material 1: The CCDC number 2203973 for the compound **1** has crystallographic supplementary data and can be obtained without paying any charge from http://www.ccdc.cam.ac.uk/conts/retrieving.html (accessed on 1 October 2022), or the Cambridge Crystallographic Data Center, 12 Union Road, Cambridge CB2 1EZ, UK; fax: (+44) 1223-336-033; or e-mail: deposit@ccdc.cam.ac.uk. The supplementary data include IR spectra in Figures S1–S4 respectively for the ligand and the complexes **1**–**3**; ^{1}H NMR and ^{13}C NMR spectra of compounds in Figures S5–S10; molecular packing and fingerprint plots from Hirshfeld surface analysis for the X-ray structure **1** in Figure S11 and S12, respectively.

Author Contributions: Conceptualization and visualization, P.D. (Pratima Debnath) and M.R.; investigation, P.D. (Pratima Debnath), M.R. and T.K.M.; data curation, P.D. (Pratima Debnath), P.D. (Paresh Debnath), M.R., T.K.M., L.S., W.M., T.A., D.M. and A.S.N.; writing-original draft preparation, P.D. (Pratima Debnath), P.D. (Paresh Debnath), M.R., T.K.M., D.M., W.M., and A.S.N.; writing-review and editing, P.D., M.R., T.K.M., W.M., and A.S.N.; supervision, M.R. and T.K.M. All authors have read and agreed to the published version of the manuscript.

Funding: This research received no external funding.

Data Availability Statement: Not applicable.

Acknowledgments: We thank Department of Chemistry, NIT Agartala for providing research facilities. PB is grateful to NIT Agartala for receiving institutional fellowship from MHRD, Govt. of India. The DFT calculations, topological analysis of the electron density distribution, and Hirshfeld surface analysis were supported by the RUDN University Strategic Academic Leadership Program. We would like to thank SAIF, IISC Bangalore for NMR studies. Moreover, all authors in this section have consented to the acknowledgements.

Conflicts of Interest: All authors declare that there are no conflict of interests on this research work.

References

1. Saxena, A.K. Organotin compounds: Toxicology and biomedicinal applications. *Appl. Organomet. Chem.* **1987**, *1*, 39–56. [CrossRef]
2. Ghazi, D.; Rasheed, Z.; Yousif, E. Review of organotin compounds: Chemistry and applications. *Int. J. Res. Eng. Innov.* **2018**, *2*, 340–348.
3. Tabassum, S.; Khan, R.A.; Arjmand, F.; Sen, S.; Kayal, J.; Juvekar, A.S.; Zingde, S.M. Synthesis and characterization of glycoconjugate tin (IV) complexes: In vitro DNA binding studies, cytotoxicity, and cell death. *J. Organomet. Chem.* **2011**, *696*, 1600–1608. [CrossRef]
4. Arjmand, F.; Jamsheera, A. Synthesis, characterization and in vitro DNA binding studies of tin (IV) complexes of tert-butyl 1-(2-hydroxy-1-phenylethylamino)-3-methyl-1-oxobutan-2-yl carbamate. *J. Organomet. Chem.* **2011**, *696*, 3572–3579. [CrossRef]
5. Paul, A.; Hazra, S.; Guedes da Silva, M.F.C.; Pombeiro, A.J. Biological Evaluation of Azo-and Imino-Based Carboxylate Triphenyltin (IV) Compounds. *Eur. J. Inorg. Chem.* **2020**, *11–12*, 930–941. [CrossRef]
6. Amir, M.K.; Khan, S.; Shah, A.; Butler, I.S. Anticancer activity of organotin (IV) carboxylates. *Inorg. Chim. Acta* **2014**, *423*, 14–25. [CrossRef]
7. Devi, J. Pachwania, S. Recent advancements in DNA interaction studies of organotin (IV) complexes. *Inorg. Chem. Commun.* **2018**, *91*, 44–62. [CrossRef]

8. Dahmani, M.; Harit, T.; Et-Touhami, A.; Yahyi, A.; Eddike, D.; Tillard, M.; Benabbes, R. Two novel macrocyclic organotin (IV) carboxylates based on bipyrazoledicarboxylic acid derivatives: Syntheses, crystal structures and antifungal activities. *J. Organomet. Chem.* **2021**, *948*, 121913. [CrossRef]
9. Shoaib Ahmad Shah, S.; Ashfaq, M.; Waseem, A.; Mehboob Ahmed, M.; Najam, T.; Shaheen, S.; Rivera, G. Synthesis and biological activities of organotin (IV) complexes as antitumoral and antimicrobial agents. *A Rev. Mini Rev. Med. Chem.* **2015**, *15*, 406–426. [CrossRef]
10. Debnath, P.; Singh, K.S.; Singh, K.K.; Singh, S.S.; Sieroń, L.; Maniukiewicz, W. Di-butyltin (IV) complexes with azo-carboxylates: Synthesis, characterization, crystal structures and their anti-diabetic assay. *New J. Chem.* **2020**, *44*, 5862–5872. [CrossRef]
11. Tiekink, E.R. Structural chemistry of organotin carboxylates: A review of the crystallographic literature. *Appl. Organomet. Chem.* **1991**, *5*, 1–23. [CrossRef]
12. Abbas, S.M.; Ali, S.; Hussain, S.T.; Shahzadi, S. structural diversity in organotin(IV) dithiocarboxylates and carboxylates. *J. Coord. Chem.* **2013**, *66*, 2217–2234. [CrossRef]
13. Nath, M.; Saini, P.K. Chemistry and applications of organotin (IV) complexes of Schiff bases. *Dalton Trans.* **2011**, *40*, 7077–7121. [CrossRef] [PubMed]
14. Basu, S.; Masharing, C.; Das, B. Diorganotin (IV) complexes of polyaromatic azo-azomethine ligand derived from salicylaldehyde and ortho-aminophenol: Synthesis, characterization, and molecular structures. *Heteroat. Chem.* **2012**, *23*, 457–465. [CrossRef]
15. Debnath, P.; Das, A.; Singh, K.S.; Yama, T.; Singh, S.S.; Butcher, R.J.; Maniukiewicz, W. Synthesis, structural characterization and antimicrobial activities of triorganotin (IV) azo-carboxylates derived from ortho/para-amino benzoic acids and β-naphthol. *Inorg. Chim. Acta.* **2019**, *498*, 119172. [CrossRef]
16. Debnath, P.; Singh, K.S.; Devi, T.S.; Singh, S.S.; Butcher, R.J.; Sieroń, L.; Maniukiewicz, W. Synthesis, characterization, crystal structures and anti-diabetic activity of organotin (IV) complexes with 2-(4-hydroxynaphthylazo)-benzoic acid. *Inorg. Chim. Acta.* **2020**, *510*, 119736. [CrossRef]
17. Debnath, P.; Singh, K.S.; Sharma, S.; Debnath, P.; Singh, S.S.; Sieroń, L.; Maniukiewicz, W. Synthesis, structural characterization, Hirshfeld surface analysis and in vitro-antimicrobial activities of triphenyltin (IV) compounds of azo-carboxylates derived from 2-or 4-amino benzoic acids and naphthalen-1 or 2-ol. *J. Mol. Struct.* **2021**, *1223*, 128971. [CrossRef]
18. Yin, H.D.; Chen, S.W. Synthesis and characterization of di-and tri-organotin (IV) complexes with Schiff base ligand pyruvic acid 3-hydroxy-2-naphthoyl hydrazone. *Inorg. Chim. Acta.* **2006**, *359*, 3330–3338. [CrossRef]
19. BasuBaul, T.S.; Basu, S.; de Vos, D.; Linden, A. Amino acetate functionalized Schiff base organotin (IV) complexes as anticancer drugs: Synthesis, structural characterization, and in vitro cytotoxicity studies. *Investig. New Drugs.* **2009**, *27*, 419–431. [CrossRef]
20. Yin, H.; Liu, H.; Hong, M. Synthesis, structural characterization and DNA-binding properties of organotin (IV) complexes based on Schiff base ligands derived from 2-hydroxy-1-naphthaldy and 3-or 4-aminobenzoic acid. *J. Organomet. Chem.* **2012**, *713*, 11–19. [CrossRef]
21. Roy, M.; Roy, S.; Devi, N.M.; Singh, C.B.; Singh, K.S. Synthesis, structural characterization and antimicrobial activities of diorganotin (IV) complexes with azo-imino carboxylic acid ligand: Crystal structure and topological study of a doubly phenoxide-bridged dimeric dimethyltin (IV) complex appended with free carboxylic acid groups. *J. Mol. Struct.* **2016**, *1119*, 64–70.
22. Baul, T.S.B.; Addepalli, M.R.; Lyčka, A.; van Terwingen, S.; da Silva, M.F.C.G. Synthesis and structural characterization of diorganotin (IV) complexes with heteroditopic pyridyl-ONO′-ligands. *Inorg. Chim. Acta.* **2020**, *512*, 119892. [CrossRef]
23. BasuBaul, T.S.; Chaurasiya, A.; Rabha, M.; Khatua, S.; Lyčka, A.; Schollmeyer, D.; Jurkschat, K. Diorganotin Compounds Containing α-Aminoacidato Schiff Base Ligands Derived from Functionalized 2-Hydroxy-5-(aryldiazenyl) benzaldehyde. Syntheses, Structures and Sensing of Hydrogen Sulfide. *Eur. J. Inorg. Chem.* **2020**, *18*, 1803–1813. [CrossRef]
24. BasuBaul, T.S.; Addepalli, M.R.; Duthie, A.; Singh, P.; Koch, B.; Gildenast, H.; Englert, U.; Rojas-León, I.; Höpfl, H. Triorganotin (IV) derivatives with semirigid heteroditopic hydroxo-carboxylato ligands: Synthesis, characterization, and cytotoxic properties. *Appl. Organomet. Chem.* **2021**, *35*, E608.
25. Roy, M.; Roy, S.; Singh, K.S.; Kalita, J.; Singh, S.S. Synthesis, characterisation and anti-diabetic activities of triorganotin (IV) azo-carboxylates derived from amino benzoic acids and resorcinol: Crystal structure and topological study of a 48 membered macrocyclic-tetrameric trimethyltin (IV) complex. *Inorg. Chim. Acta.* **2016**, *439*, 164–172. [CrossRef]
26. Chen, L.; Wang, Z.; Qiu, T.; Sun, R.; Zhao, Z.; Tian, L.; Liu, X. Synthesis, structural characterization, and properties of triorganotin complexes of Schiff base derived from 3-aminobenzoic acid and salicylaldehyde or 2, 4-pentanedione. *Appl. Organomet. Chem.* **2020**, *34*, E5790. [CrossRef]
27. BasuBaul, T.S.; Chaurasiya, A.; Duthie, A.; Montes-Tolentino, P.; Höpfl, H. Coordination-driven self-assembly of macrocycles and 1D or 2D coordination polymers using heteroditopic pyridyl-carboxylate ligands: The case study of 5-[(E)-2-(3-pyridyl)-1-diazenyl]-2-hydroxybenzoate in combination with $\{R_nSn\}$(n= 2 and 3). *Cryst. Growth Des.* **2019**, *19*, 6656–6671. [CrossRef]
28. BasuBaul, T.S.; Das, P.; Eng, G.; Linden, A. Synthesis and Characterization of Some Triphenyltin (IV) Complexes from Sterically Crowded [((E)-1-{2-Hydroxy-5-[(E)-2-(aryl)-1-diazenyl] phenyl} methylidene) amino] acetate Ligands and Crystal Structure Analysis of a Tetrameric Triphenyltin (IV) Compound. *J. Inorg. Organomet. Polym. Mater.* **2010**, *20*, 134–141. [CrossRef]
29. Baul, T.S.B.; Singh, K.S.; Holčapek, M.; Jirásko, R.; Rivarola, E.; Linden, A. Synthesis, characterization and crystal structures of polymeric and dimeric triphenyltin (IV) complexes of 4-[((E)-1-{2-hydroxy-5-[(E)-2-(2-carboxyphenyl)-1-diazenyl] phenyl} methylidene) amino] aryls. *J. Organomet. Chem.* **2005**, *690*, 4232–4242. [CrossRef]

30. Singh, K.S.; Roy, M.; Roy, S.; Ghosh, B.; Devi, N.M.; Singh, C.B.; Mun, L.K. Synthesis, characterization and antimicrobial activities of triorganotin (IV) complexes with azo-azomethine carboxylate ligands: Crystal structure of a tributyltin (IV) and a trimethyltin (IV) complex. *J. Coord. Chem.* **2017**, *70*, 361–380. [CrossRef]
31. Shang, X.; Cui, J.; Wu, J.; Pombeiro, A.J.L.; Li, Q. Polynuclear diorganotin (IV) complexes with arylhydroxamates: Syntheses, structures and in vitro cytotoxic activities. *J. Inorg. Biochem.* **2008**, *102*, 901–909. [CrossRef] [PubMed]
32. Rigaku, O.D. *CrysAlis PRO*; Rigaku Oxford Diffraction Ltd.: Yarnton, UK, 2019.
33. Sheldrick, G.M. SHELXT—Integrated space-group and crystal-structure determination. *Acta Cryst.* **2015**, *A 71*, 3–8. [CrossRef]
34. Sheldrick, G.M. Crystal structure refinement with SHELXL. *Acta Cryst.* **2015**, *C 71*, 3–8.
35. Wolff, S.K.; Grimwood, D.J.; McKinnon, J.J.; Turner, M.J.; Jayatilaka, D.; Spackman, M.A. *Crystal Explorer (Version 3.1)*; University of Western Australia: Nedland, Australia, 2012.
36. Spackman, M.A.; Jayatilaka, D. Hirshfeld surface analysis. *Cryst. Eng. Comm.* **2009**, *11*, 19–32. [CrossRef]
37. McKinnon, J.J.; Jayatilaka, D.; Spackman, M.A. Towards quantitative analysis of intermolecular interactions with Hirshfeld surfaces. *Chem. Commun.* **2007**, 3814–3816. [CrossRef] [PubMed]
38. Bondi, A. Van der Waals volumes and radii of metals in covalent compounds. *J. Phys. Chem.* **1966**, *70*, 3006–3007. [CrossRef]
39. Chai, J.D.; Head-Gordon, M. Long-range corrected hybrid density functionals with damped atom–atom dispersion corrections. *Phys. Chem. Chem. Phys.* **2008**, *10*, 6615–6620. [CrossRef]
40. Frisch, M.J.; Trucks, G.W.; Schlegel, H.B.; Scuseria, G.E.; Robb, M.A.; Cheeseman, J.R.; Scalmani, G.; Barone, V.; Mennucci, B.; Petersson, G.A.; et al. *Fox, in Gaussian 09, Revision C.01*; Gaussian, Inc.: Wallingford, CT, USA, 2010.
41. Barros, C.L.; De Oliveira, P.J.P.; Jorge, F.E.; Canal Neto, A.; Campos, M. Gaussian basis set of double zeta quality for atoms Rb through Xe: Application in non-relativistic and relativistic calculations of atomic and molecular properties. *Mol. Phys.* **2010**, *108*, 1965–1972. [CrossRef]
42. Jorge, F.E.; Canal Neto, A.; Camiletti, G.G.; Machado, S.F. Contracted Gaussian basis sets for Douglas–Kroll–Hess calculations: Estimating scalar relativistic effects of some atomic and molecular properties. *J. Chem. Phys.* **2009**, *130*, 064108. [CrossRef]
43. Neto, A.C.; Jorge, F.E. All-electron double zeta basis sets for the most fifth-row atoms: Application in DFT spectroscopic constant calculations. *Chem. Phys. Lett.* **2013**, *582*, 158–162. [CrossRef]
44. De Berrêdo, R.C.; Jorge, F.E. All-electron double zeta basis sets for platinum: Estimating scalar relativistic effects on platinum (II) anticancer drugs. *J. Mol. Struc-THEOCHEM.* **2010**, *961*, 107–112. [CrossRef]
45. Lu, T.; Chen, F. Multiwfn: A multifunctional wavefunction analyzer. *J. Comput. Chem.* **2012**, *33*, 580–592. [CrossRef] [PubMed]
46. Bauer, A.W.; Kirby, W.M.M.; Sherris, J.C.; Turck, M. Antibiotic susceptibility testing by a standardized single disk method. *Am. J. Clin. Pathol.* **1966**, *45*, 493–496. [CrossRef] [PubMed]
47. Addison, A.W.; Rao, T.N.; Reedijk, J.; van Rijn, J.; Verschoor, G.C. Synthesis, structure, and spectroscopic properties of copper(II) compounds containing nitrogen–sulphur donor ligands; the crystal and molecular structure of aqua [1,7-bis(N-methylbenzimidazol-2′-yl)-2,6-dithiaheptane]copper(II) perchlorate. *J. Chem. Soc. Dalt. Trans.* **1984**, 1349–1356. [CrossRef]
48. Espinosa, E.; Alkorta, I.; Elguero, J.; Molins, E. From weak to strong interactions: A comprehensive analysis of the topological and energetic properties of the electron density distribution involving X–H$\cdots$ F–Y systems. *J. Chem. Phys.* **2002**, *117*, 5529–5542. [CrossRef]
49. Johnson, E.R.; Keinan, S.; Mori-Sánchez, P.; Contreras-García, J.; Cohen, A.J.; Yang, W. Revealing noncovalent interactions. *J. Am. Chem. Soc.* **2010**, *132*, 6498–6506. [CrossRef]
50. Contreras-García, J.; Johnson, E.R.; Keinan, S.; Chaudret, R.; Piquemal, J.P.; Beratan, D.N.; Yang, W. NCIPLOT: A program for plotting noncovalent interaction regions. *J. Chem. Theory Comput.* **2011**, *7*, 625–632. [CrossRef]